




ZTIFs derived nitrogen-introduced high specific area and hierarchical porous carbon for oxygen reduction reaction

Jizhao Zou^{1,2}, Minggui Peng^{1,2} , Peng Liu^{1,2}, Shengjiao Zhang^{1,2}, Qi Zhang^{3,4}, Fei Deng⁵, Xierong Zeng^{1,2}, and Xiaohua Li^{1,2,*}

¹ Shenzhen Key Laboratory of Special Functional Materials, Shenzhen University, Shenzhen 518060, China

² Shenzhen Engineering Laboratory for Advance Technology of Ceramics, College of Materials Science and Engineering, Shenzhen University, Shenzhen 518060, China

³ BCMaterials, Basque Center for Materials, Applications and Nanostructures, UPV/EHU Science Park, 48940 Leioa, Spain

⁴ IKERBASQUE, Basque Foundation for Science, Plaza Euskadi, 5, 48009 Bilbao, Spain

⁵ Government Invest, & Develop Projects Evaluation Center, Development and Reform Bureau, Pingshan District, Shenzhen, China

Received: 3 March 2021

Accepted: 22 April 2021

Published online:

19 June 2021

© The Author(s), under exclusive licence to Springer Science+Business Media, LLC, part of Springer Nature 2021

ABSTRACT

It is of great allure to construct nitrogen-doped hierarchical porous carbon to replace Pt-based catalysts for efficient ORR. Here, nitrogen-doped hierarchical porous carbon (NHPC) was prepared by carbonizing ZTIF-1 and KOH activating. The resultant NHPC4-700 catalyst exhibits a hierarchical porous structure and high specific area ($2404 \text{ m}^2 \text{ g}^{-1}$), which promoted the exposure of enough active sites as well as simultaneously enhanced the electron transfer rate, shorten the mass transfer pathway, enhanced ionic conductivity and carbon wetting. The results are capable of remarkably improving the ORR activities of carbon materials. The NHPC4-700 catalyst exhibits a great catalytic performance with onset potential at 0.90 V and limiting current density of -6.0 mA cm^{-2} , which is close to commercial Pt/C electrocatalyst. Meanwhile, the NHPC4-700 catalysts had better stability and methanol resistance than that of Pt/C toward ORR. These superior electrochemical properties of the NHPC4-700 catalysts were closely related to their nitrogen-doped hierarchical porous structure and high specific area.

Address correspondence to E-mail: lxh@szu.edu.cn

1 Introduction

In recent years, the energy crisis and environmental pollution caused using fossil fuels have forced us to explore new energy system to replace them, and create efficient energy-storage devices. As we all know, hydrogen energy is an ideal substitute for traditional fossil fuels due to its high energy density and environmentally friendly reaction product [1, 2]. Oxygen reduction reaction (ORR) is a crucial cathodic reaction in a hydrogen energy system. However, the acceleration of sluggish kinetics acquires efficient electrocatalysts to make cathodic reaction fast enough for applications [3]. Among all the electrocatalysts, precious metal catalysts especially platinum-based materials are widely used as fuel cell cathodic electrocatalysts because of their excellent ORR activity [4, 5]. However, the high cost, poor stability and methanol crossover effect seriously hindered their applications [6–8]. Therefore, it is necessary to develop a cheap and stable substitute to replace those precious metals-derived electrocatalysts.

Carbon-based materials are widely used for energy-storage devices due to their adjustable porous structure, high specific area, abundant sources and superior chemical stability [9–15]. However, pure carbon materials usually deliver an unsatisfactory electrocatalytic performance, which is not satisfactory for the catalytic activity of electrochemical ORR. Recently, heteroatoms-decorated (N, O, P, F, etc.) carbon materials have been further investigated and are considered as the promising substitute for ORR [16–22]. Among them, nitrogen-doped materials are the most widely investigated heteroatom-decorated carbons, because the nitrogen atoms can activate their neighboring carbon atoms during ORR process. However, the superior ORR catalytic activity in alkaline media is due to the nitrogen dopants including quaternary-N, which is beneficial for the limiting current density, and pyridinic-N that could decrease the adsorption energy of O₂ at electrode surface resulting in a positive onset potential [23]. Meanwhile, it is very important to control the structure and morphology of materials during the whole synthesis process, but the goal is still a challenge in the modern scientific and industrial studies [24–28]. Additionally, recent research has found that metal-organic frameworks (MOFs) derived materials can provide high specific surface area and porous

structure which promote mass transfer and create more active sites [29–32]. Qian et al. pyrolyzed a Zn-MOF and obtained a highly porous B-N dual-doped carbon which exhibited an onset potential of 0.894 V (vs. RHE) and a current density of 4.73 mA cm⁻². However, the carbon material obtained from a simple carbonization of MOFs has less mesopore structure, which is not beneficial for mass transfer resulting in a poor ORR performance. However, a series of materials with a hierarchical porous structure have gained great interest in energy, catalysis, environment etc. [33]. In particular, micropore can as a confined reactor and expose enough active sites [34]. Meanwhile, mesopore and macropore could simultaneously enhance the electron transfer rate, shorten the mass transfer pathway, enhanced ionic conductivity and carbon wetting, which are capable of remarkably improving the ORR activities of carbon materials in both acid and alkaline condition [35]. In addition, higher specific surface area can expose more active sites, thus improving the electrochemical catalytic activity of ORR [36]. Therefore, it is important to synthesize nitrogen-doped hierarchical porous carbon materials with high specific surface area [37]. In order to obtain hierarchical porous carbon materials, chemical activation methods are often used to develop the pore network structure of carbon materials [38]. This method is usually carried out by mixing the chemical activating agents (such as KOH etc.) with carbon precursors at different mass-ratios and temperatures. The specific area can be greatly increased and a large number of mesopore and macropore structures can be obtained [39]. Zhang et al. mixed the cellulose with KOH to obtain a defect-rich graphene-like nanocarbon material which can get an onset potential of 0.991 V and a current density of 5.6 mA cm⁻² [40]. However, KOH activation leads to a great loss of nitrogen. In order to preserve more nitrogen after the activation, ZTIF-1 that contains 5-methyltetrazole is used as the precursor that can preserve enough nitrogen content for ORR after KOH activation.

In this study, we developed a nitrogen-doped hierarchical porous carbon (NHPC) with rich defects, hierarchical porous structure and dominant pyridinic-N and pyrrolic-N content by carbonizing ZTIFs (zeolitic tetrazolate-imidazolate frameworks) and activating the carbonized-products. During the activation, the violent reaction produced metallic K, K₂O and CO₂ and hydrogen gas. The K₂O will be embed

into carbon layers and the released gases (H_2 , H_2O , CO_2 , CO , etc.) will leave a large number of pores as well as defects which can promote mass transfer and catalytic activity. The prepared NHPC had a large specific area of $2404 \text{ m}^2 \text{ g}^{-1}$ and a great number of mesopores leading to a hierarchical porous structure. The NHPCs were used as ORR electrocatalyst in 0.1 M KOH solution and exhibited an excellent electrocatalytic performance. The NHPC4-700 shows an onset potential of 0.90 V, and limiting current density of -6.0 mA cm^{-2} which is close to the commercial 20% Pt/C material (onset potential of 0.97 V and limiting current density of 5.46 mA cm^{-2}). With further investigation, NHPC4-700 has a better durability and methanol tolerance performance. Hence, we believe that NHPC4-700 can become an ideal substitute to Pt/C.

2 Experimental

2.1 Materials

Zinc acetate ($Zn(CH_3CO_2)_2$), ethanol and 5-methyltetrazole were purchased from Macklin. *N,N*-Dimethylformamide (DMF) and potassium hydroxide was purchased from Aladdin. 2-ethylimidazole was purchased from TCI. All chemical reagents were of analytical grade and used without any further purification.

2.2 Synthesis of NHPC

The zeolitic tetrazolate-imidazolate frameworks (ZTIF-1) was prepared by following the method [41]. 0.96 g 2-ethylimidazole, 1.83 g zinc acetate and 0.86 g 5-methyltetrazole were dissolved in the mixture of 50 mL DMF and 50 mL ethanol. The mixture was sealed in a 250 mL hydrothermal reactor and heated at $120 \text{ }^\circ\text{C}$ for 72 h, then cooled to room temperature. The yellow crystals (ZTIF-1) was collected through filtered and washed with ethanol, and dried 12 h at $70 \text{ }^\circ\text{C}$.

The NHPC is synthesized by the following process. Firstly, ZTIF-1 was carbonized at $800 \text{ }^\circ\text{C}$ under Ar atmosphere for 2 h with a rate of $10 \text{ }^\circ\text{C min}^{-1}$ to gain nitrogen-decorated nanoporous carbon (NNPC) [42]. Secondly, the resultant NNPC was chemically activated with KOH. For this purpose, the NNPC was mixed with KOH at different mass ratio (1:1, 1:2, 1:3

and 1:4) and reacted at different temperatures ($700 \text{ }^\circ\text{C}$, $750 \text{ }^\circ\text{C}$ and $800 \text{ }^\circ\text{C}$) under Ar atmosphere for 1 h with a rate of $5 \text{ }^\circ\text{C min}^{-1}$. Finally, these samples were washed with diluted sulfuric acid (20 wt%) and deionized water to totally remove KOH and other ions, and dried 12 h at $70 \text{ }^\circ\text{C}$. The resultant samples were named as NHPCx-T (x represents the KOH/NHPC mass ratio and T represents the reacting temperature), respectively.

2.3 Characterization

Field emission scanning electron microscopy (FESEM) images were acquired by a Hitachi SU-70 FESEM instrument. X-ray diffraction (XRD) patterns were collected by a Bruker D8 Advance powder X-ray diffractometer using $Cu \text{ K}\alpha$ radiation. The specific surface area is obtained by using micromeritics ASAP 2020 analyzer based on the Brunauer-Emmett-Teller (BET) method. Raman spectra was performed on RENISHAW inVia Raman Microscope. X-ray photoelectron spectroscopy (XPS) measurements were carried out on Microlab 350. Element analysis was carried out on Vario EL cube.

2.4 Electrochemical measurements

Electrochemical measurements were carried out at room temperature on a Bio-logic VMP-300 electrochemistry workstation together with a PINE rotating ring-disk electrode (RRDE). For ORR testing, 1.0 mg active material was firstly dispersed in a Nafion/methanol solution (100 μL , 0.25% Nafion) by sonication for 0.5 h and therefore a well-dispersed catalyst ink was obtained. Then, to load the catalyst onto electrode, 10 μL ink was injected onto the glassy-carbon electrode and dried in air. The ORR activity of all materials was examined by rotating ring-disk electrode (RRDE) measurements. The number of transferred electrons during ORR was analyzed according to Koutecky–Levich (K–L) equation [43], as shown below:

$$\frac{1}{J} = \frac{1}{J_L} + \frac{1}{J_K} = \frac{1}{B\omega^{1/2}} + \frac{1}{J_K}$$

$$B = 0.62nFC_0D_O^{2/3}v^{-1/6}$$

$$J_K = nFkC_0$$

where J is the measured current density, J_L the diffusion current density, J_K the kinetic limiting current

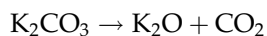
density, ω the angular velocity, n is electron transfer number, F the Faraday constant ($96,485 \text{ C mol}^{-1}$), D_0 the diffusion coefficient of O_2 in the electrolyte ($1.9 \times 10^{-5} \text{ cm}^2 \text{ s}^{-1}$), ν the kinematic viscosity of the electrolyte ($0.01 \text{ cm}^2 \text{ s}^{-1}$), and C_0 the bulk concentration of O_2 in the 0.1 M KOH electrolyte.

3 Results and discussion

In this work, the synthesis process of NHPC is illustrated in scheme 1. First, the ZTIF-1 was synthesized by a one-step hydrothermal process. The introduction of 5-methyltetrazole not only provides the ligand of ZTIF-1 but also brings out a high in situ N content. After pyrolysis and acid wash, the product is referred to NNPC. Last, KOH activation is carried out to create a hierarchical porous structure and then NHPC is obtained. During the activation, the violent reaction produced metallic K, K_2CO_3 and hydrogen gas based on the following equation: [39]



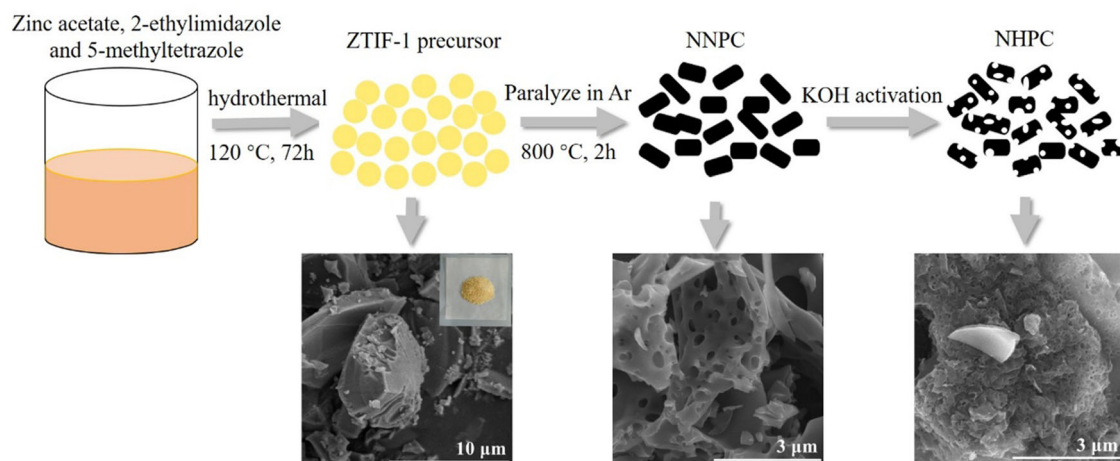
The as produced K compounds can corrode the carbon layers to form abundant edges and defects in NHPC. K_2CO_3 will be further decomposed into K_2O and CO_2 following the equation. The K_2O will be embed into carbon layers and the released gases (H_2 , H_2O , CO_2 , CO , etc.) will leave a large number of pores as well as defects which can promote mass transfer and catalytic activity.



The XRD pattern of ZTIF-1 is shown in the Fig. 1a, which shows the typical structure of ZTIF-1 [42]. Figure 1b shows the XRD pattern of NNPC and NHPC4-700. NNPC has two broad peaks at 24° and 44° (2θ) which are corresponding to (002) and (100) diffraction peaks of carbon (PDF#03-0401), respectively. After the KOH activation process, the pattern of NHPC4-700 reveals the (002) diffraction peak decreasing apparently. The results show that KOH activation leads to a limited degree of graphitization. However, the formation of a large number of disordered carbon structures increases the defect and specific surface area (SSA).

Raman spectra for NNPC and different NHPCs are shown in Fig. 2a, b. The peak at around 1340 cm^{-1} relates to D band which stands for disordered carbon and defected carbon. The peak at around 1580 cm^{-1} relates to G band which stands for graphitic carbon. The intensity ratio of two peaks (I_D/I_G) reveals the graphitization degree of carbon material. The I_D/I_G ratio of NHPC2-700, NHPC3-700 and NHPC4-700 is 0.91, 0.92 and 0.93, respectively. It reveals that NHPC will get more defects by increasing KOH mass ratio. The I_D/I_G ratio of NHPC3-700, NHPC3-750 and NHPC3-800 is 0.92, 0.95 and 0.98, respectively. This demonstrates that increasing activation temperature will promote activation reaction and reduce the graphitization degree of NHPC.

The network structures are further validated by SEM (Fig. 3a–c), TEM (Fig. 3d–e) and HR-TEM (Fig. S1b–f). Figure 3a–c shows the SEM images of ZTIF-1, NNPC and NHPC. By comparison, it can be found that carbonization makes NNPC get many porous



Scheme 1 The synthesis process of NHPC

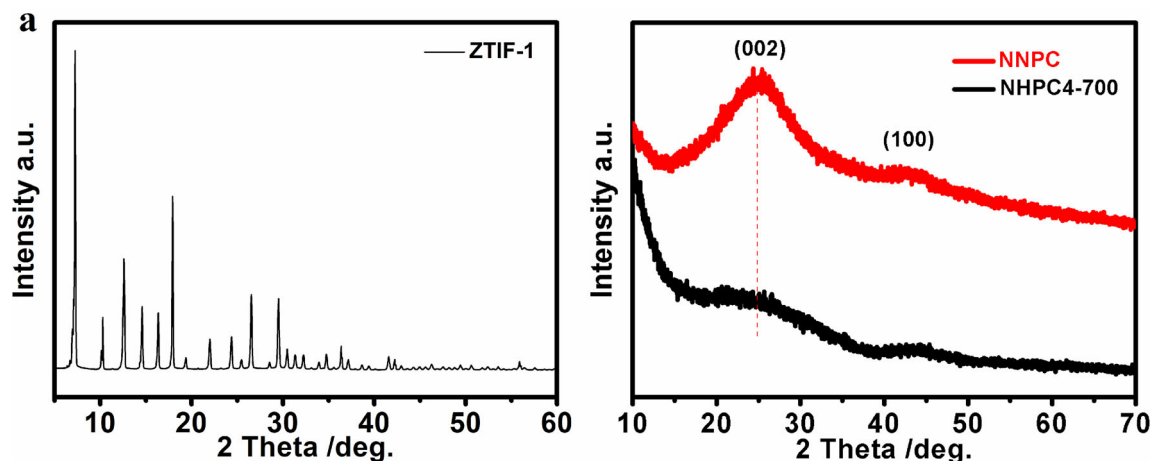


Fig. 1 XRD patterns of a ZTIF-1 and b NNPC and NHPC4-700

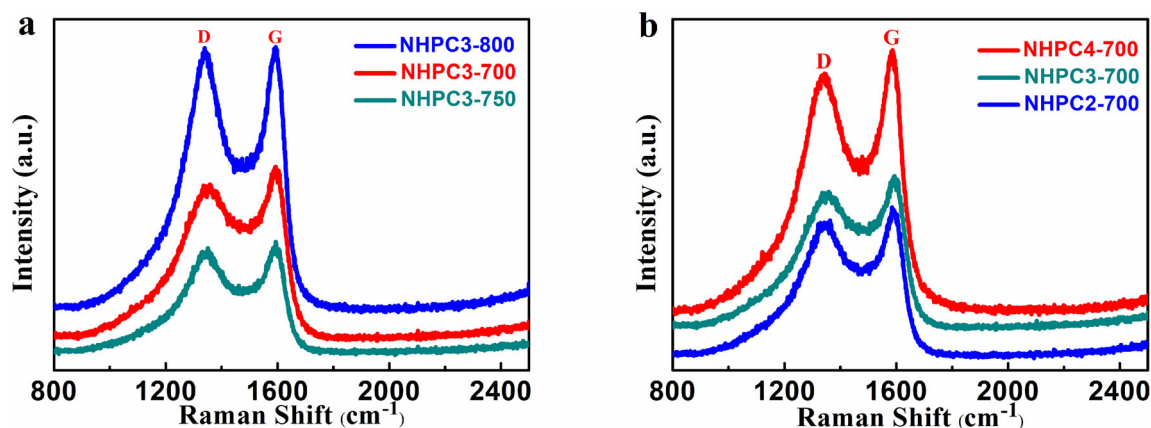


Fig. 2 Raman shifts of a NHPC3-700, NHPC3-750 and NHPC3-800 and b NHPC2-700, NHPC3-700 and NHPC4-700

structures on the basis of ZTIF-1, and the surface of NNPC is relatively smooth. By comparing NNPC and NHPC, it can be found that more pores have been added to NHPC. Under the corrosion of KOH, obvious microcracks appear on the surface, leading to the formation of mesoporous structures. At the same time, the carbon matrix shrinks and forms folds inside the NHPC, which increases the specific surface area. As a result, NHPC has abundant pore structure and ultra-high specific surface area.

The TEM images of NHPC4-700 are shown in Fig. 3d. It can be observed that there are many mesoporous and macroporous and the entire material has an irregular morphology. The HR-TEM image of NHPC4-700 (Fig. 3e and Fig. S1b–f) shows an enlarged image of a part of the area in Fig. 3d. No obvious lattice is observed, indicating that a large number of defects and microporous structures are distributed on the surface, which is consistent with

the results of average pore size distribution of BET analysis. The result NHPC4-700 catalyst provides a high specific surface area and hierarchical porous structure, which is conducive to the exposure of more active sites and improving the catalytic activity of ORR. Obviously, the KOH activation creates a large number of defects and a hierarchical porous structure was formed. Figure 3f–j shows the EDS image of NHPC4-700 and it reveals that the material is mainly composed of three elements (C, N, and O). The N element is evenly distributed in NHPC4-700, which is beneficial to improve ORR activity.

In order to further investigate the chemical composition, X-ray spectroscopic (XPS) measurements and element analysis were carried out. As shown in Fig. 4a, the spectra of NHPC4-700 reveals the existence of C, N and O content, which has the same results with TEM element mapping. Table 1 is the detailed of the element content for NNPC and

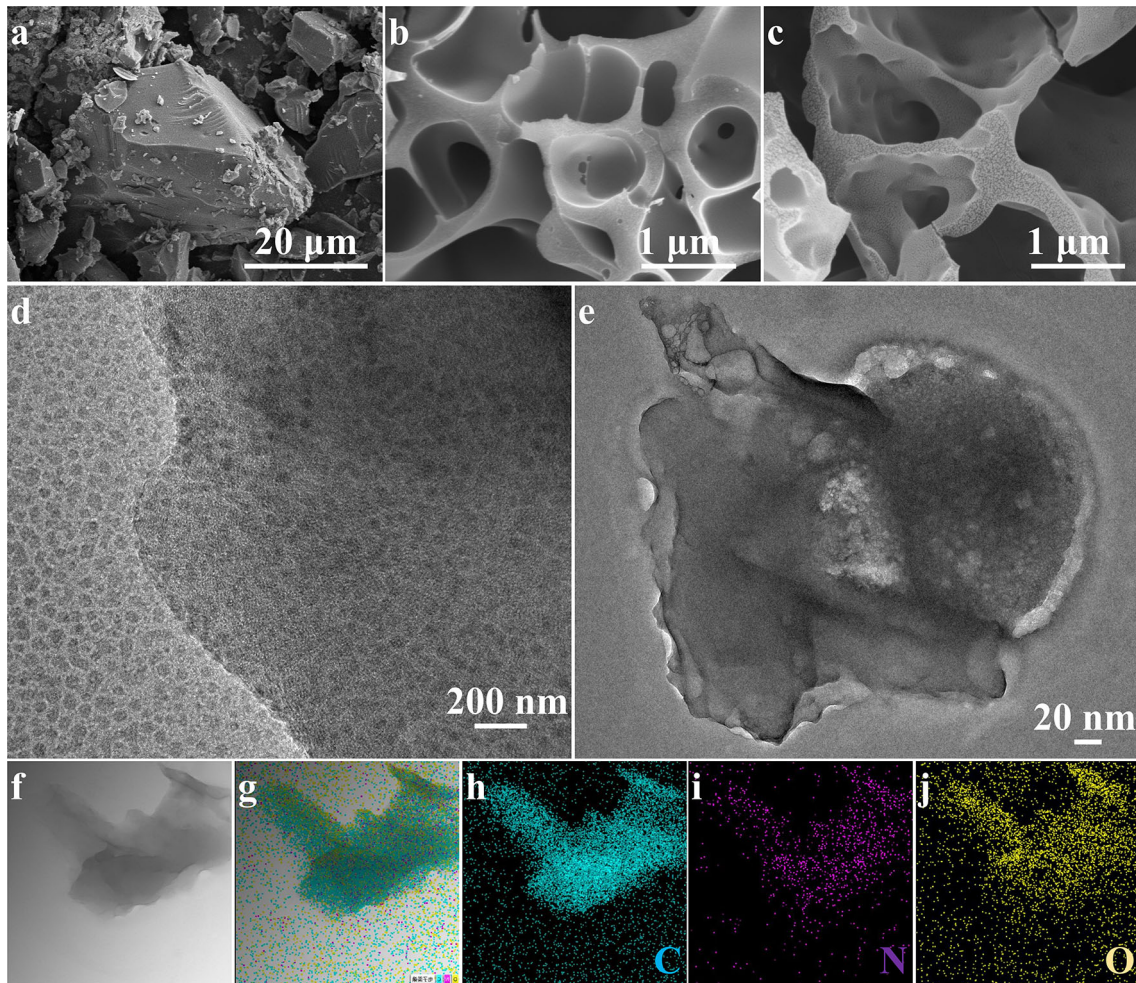


Fig. 3 SEM images of **a** ZTIF-1, **b** NNPC and **c** NHPC4-700, **d**) TEM image of NHPC4-700 and **e** HRTEM image of NHPC4-700, **f–j** element mapping of the selected area of NHPC4-700 revealing the elemental distribution of C, N and O

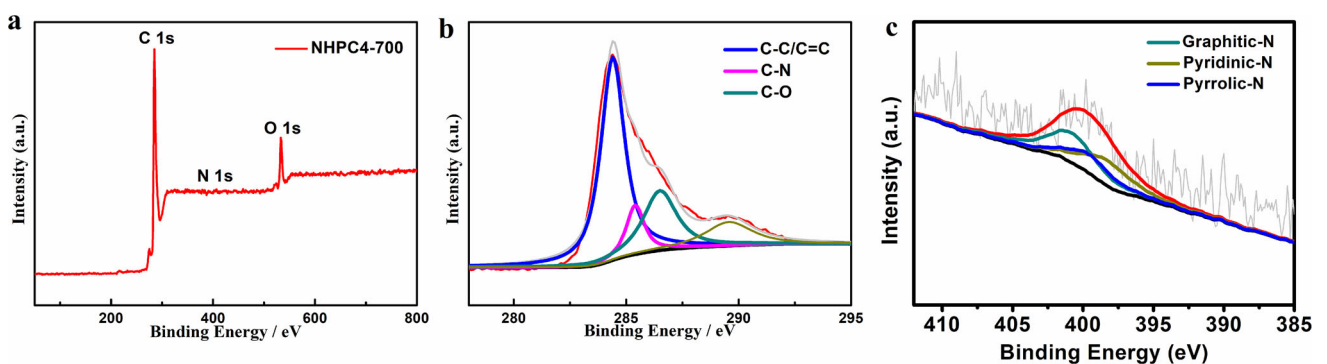


Fig. 4 XPS results of NHPC4-700 **a** XPS survey, **b** high-resolution C 1s spectra and **c** high-resolution N 1s spectra

NHPC4-700 by using organic element analyzer. The results showed that the high nitrogen content of NNPC was 15.84% after ZTIFI-1 carbonization treatment, while the nitrogen content of NNPC remained in the range of 0.35–0.99% after activation treatment,

which was sufficient to provide ORR active sites. Figure 4b shows the high-resolution C 1s spectra. It can be divided into three peaks including C–C/C=C (284.4 eV), C–N (285.4 eV), C–O (286.5 eV). The high-resolution N 1s spectra of NHPC4-700 at 397–402 eV

Table 1 The element content of NNPC and NHPCs determined by element analysis

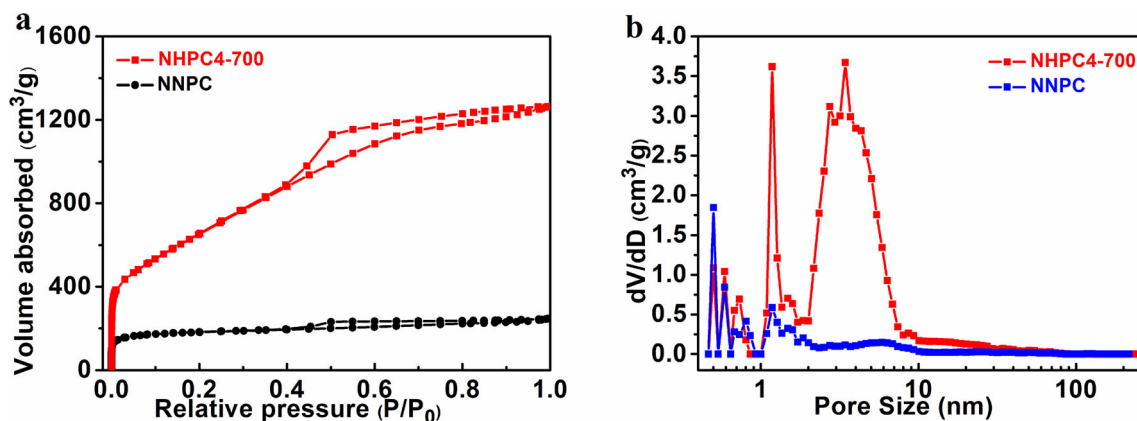
Element (wt%)	C (%)	N (%)	H (%)
NNPC	46.41	15.84	1.676
NHPC2-700	87.97	0.99	/
NHPC4-700	93.07	0.39	/
NHPC3-700	92.57	0.66	/
NHPC3-750	95.84	0.91	/
NHPC3-800	92.13	0.35	/

are shown in Fig. 4c. Each N 1s peak can be divided into three peaks corresponding to pyridinic-N ($398.3 \text{ eV} \pm 0.1 \text{ eV}$), pyrrolic-N ($399.5 \text{ eV} \pm 0.2 \text{ eV}$) and graphitic-N ($400.8 \text{ eV} \pm 0.2 \text{ eV}$). Especially, both of pyridinic-N and pyrrolic-N are beneficial for ORR. Meanwhile, they can promote the electrocatalytic performance of carbon catalyst and these two kinds of nitrogen content accounted for 60.26% of the total nitrogen content [44]. Hence, the superior catalytic activity can be attributed to the dominant pyridinic-N and pyrrolic-N content.

In order to further analyze the pore properties, nitrogen adsorption and desorption measurements are introduced to perform specific surface area (SSA) based on a BET method. Pore size is calculated by a BJH method. Figure 5a, b show the SSA and pore properties for NHPC3-700 and NNPC. Compared with the un-activated NNPC, NHPC3-700 shows a combined Type IV isotherms with a H4 hysteresis loops. As shown in Fig. 5a, the SSA of NHPC ($2404 \text{ m}^2 \text{ g}^{-1}$) is larger than NNPC ($557 \text{ m}^2 \text{ g}^{-1}$). Pore size distributions are displayed in Fig. 5b and the pore size distribution is centered at 2.64 nm.

Obviously, KOH activation makes NHPC produce more mesoporous structure, which gives it a hierarchical structure and increases SSA.

The ORR performance of NHPCs and commercial Pt/C are further studied by linear sweep voltammetry (LSV), durability and methanol tolerance test with a rotating disk electrode (RDE) device. Figure 6a, b are LSV curves of NHPCs with different activation temperature and KOH mass ratio. It is obvious that the sample heat treated at 700°C has the best electrocatalytic performance (Fig. 6a). The reason for this result is that the part of the activation reaction needs to be above 700°C [39]. With the increase of the activation temperature, the activation will be more violent. Then there will be a great loss of nitrogen (XPS table). Moreover, with the increase of temperature, the structure of NHPC will be seriously corroded, especially at 800°C activation. The great loss of nitrogen and the collapse of the carbon material structure resulted in the deterioration of the onset potential of NHPC. Therefore, 700°C is chosen as the activation temperature before studying the effect of the mass ratio of KOH. As shown in the Fig. 6b, NHPC4-700 has the best catalytic performance. The onset potential reached 0.90 V and the limiting current density was -6.0 mA cm^{-2} , which was better than other samples. When the content of KOH is too low, the activation reaction is not sufficient. Meanwhile, the pore structure is not rich enough, and the active site cannot be fully exposed. These results lead to an unsatisfactory initial potential. On the contrary, when the KOH content is too high, the intense activation process leads to the collapse of the NHPC skeleton structure, which reduces the limiting current density. As shown in the Fig. 6c, compared to

**Fig. 5** a N_2 adsorption and desorption curves and b pore distribution of NNPC and NHPC4-700

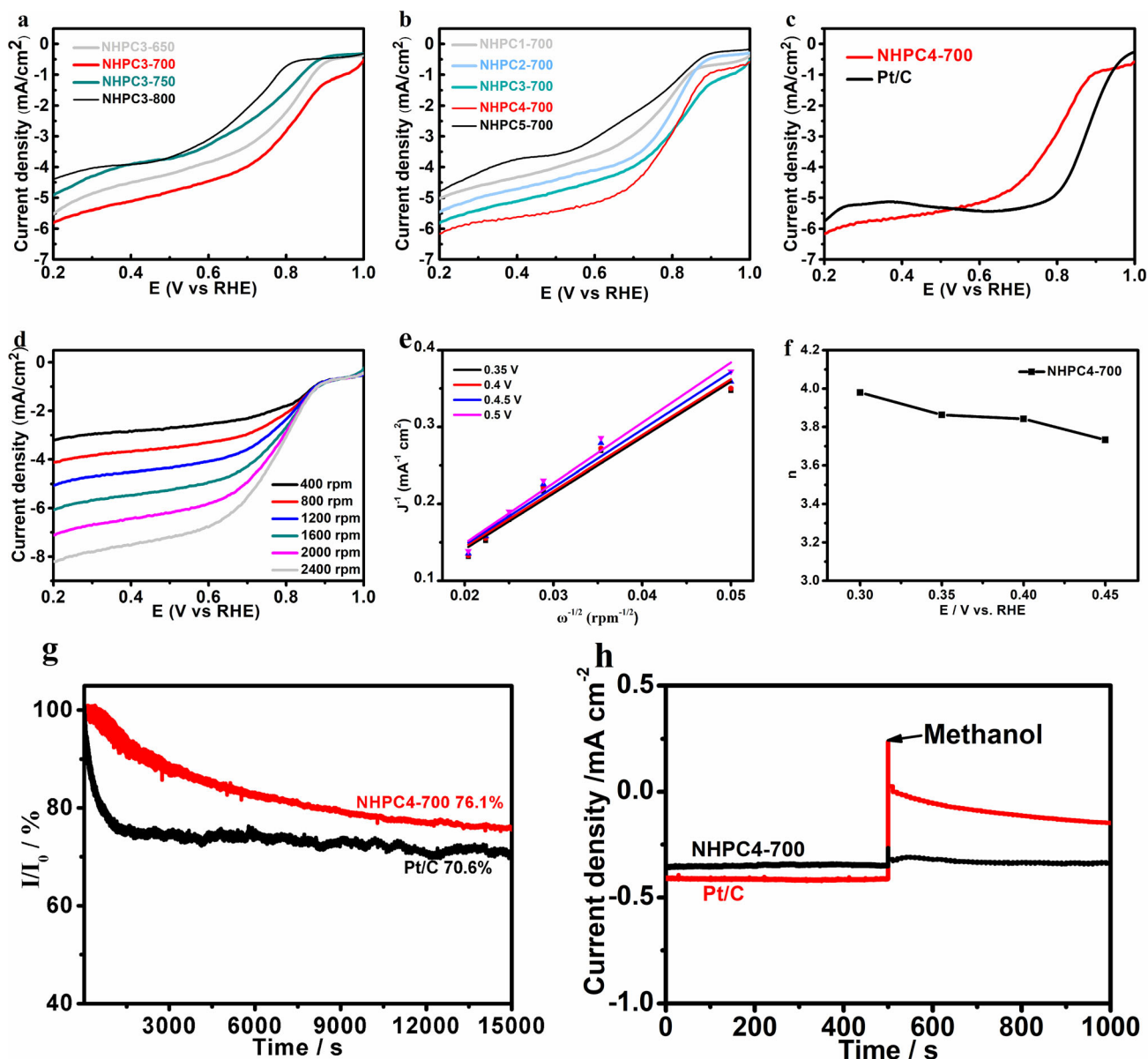


Fig. 6 **a** LSV curves of NHPC3-650, NHPC3-700, NHPC3-750 and NHPC3-3-800, **b** LSV curves of NHPC1-700, NHPC2-700, NHPC3-700, NHPC4-700 and NHPC5-700, **c** LSV curves of NHPC4-700 and Pt/C catalyst, **d** LSV curves of NHPC4-700 at different rotating rates, **e** K-L plots of NHPC4-700, **f** electron

transfer number at different potential, **g** chronoamperometric response of NHPC4-700 and Pt/C catalyst after 15,000 s and **h** chronoamperometric response of NHPC4-700 and Pt/C catalyst with the addition of 3 M methanol

commercial Pt/C, the NHPC4-700 exhibits an onset potential of 0.90 V and a half-wave potential of 0.76 V, which are close to Pt/C (0.97 V and 0.88 V, respectively) and a higher limiting current density than commercial Pt/C. As shown in Table S1, it can be observed that the ORR catalytic activity of NHPC4-700 is superior or comparable to the most recently reported metal-free catalysts. Figure 6d is the LSV curve of NHPC4-700 from 400 rpm to

2400 rpm. The limiting current density increase from -3.3 to -8.5 mA cm^{-2} . According to the Koutecky-Levich (K-L) equation, the electron transfer number of NHPC4-700 be calculated (Fig. 6e). The n values of NHPC4-700 are 3.73–3.97 (Fig. 6f), which is close to n of Pt/C. The result indicates that the reaction process of NHPC4-700 is a four-electron process. Furthermore, the LSV curve and the electron transfer number

of NHPC1-700, NHPC2-700, NHPC3-700 and NHPC5-700 are shown in Figs. S3–S4.

Herein, it is believed that the excellent electrocatalytic performance of NHPC4-700 is related to the following reasons. (i) First, the etching of the KOH activation reaction forms a hierarchical porous structure on the microporous substrate of NNPC. This hierarchical porous structure is beneficial for proton transport and the increase of limiting current density [45]. Therefore, NHPC can obtain an excellent limiting current density in comparison with Pt/C. (ii) The activation of KOH produces many defects. These defects expose active sites of nitrogen species which hidden in the material. The increase of active sites promoted the electrocatalytic activity of the NHPC catalyst and finally realized the increase of onset potential. (iii) Thirdly, based on the XPS results in Fig. 4a, it can be known that the existence of nitrogen in NHPC4-700 is mainly pyridinic-N and pyrrolic-N. As reported, pyridinic-N and pyrrolic-N can promote the electrocatalytic performance of carbon material in alkaline solution. Therefore, NHPC4-700 can obtain a better electrocatalytic performance than Pt/C in terms of limiting current density.

In addition to excellent ORR activity, it is also very important to have a good durability for electrocatalysts. Figure 6g shows the chronoamperometric current–time (*i*-*t*) measurement for NHPC4-700 and Pt/C catalysts. The *i*-*t* curves showed NHPC4-700 (76.1%) had excellent stability than that of Pt/C (70.6%) toward ORR at a constant potential of -0.4 V (vs Hg/HgO) in 0.1 M KOH. Methanol tolerance test is also carried out for NHPC4-700 and Pt/C. To evaluate the tolerance to methanol, the NHPC4-700 and Pt/C catalysts is measured in O₂-saturated 0.1 M KOH solution (1600 rpm). As shown in the Fig. 6h, after injecting 3 M methanol at 500 s, the ORR current density of NHPC4-700 keeps at the same level, while the ORR current density of Pt/C shows a strong response to methanol and then an apparent decrease for current density. This result proves that NHPC4-700 has a better methanol tolerance than that of Pt/c.

4 Conclusion

In summary, the NHPC4-700 catalyst was successfully fabricated by carbonizing ZTIF-1 process and KOH-activating approach. The resultant NHPC4-700

catalyst exhibits a hierarchical porous structure and high specific area after KOH-activating. The hierarchical porous network structure and high specific surface area (2404 m² g⁻¹) of NHPC4-700 catalyst promoted the exposure of enough active sites as well as simultaneously enhanced the electron transfer rate, shorten the mass transfer pathway, enhanced ionic conductivity and carbon wetting, which are capable of remarkably improving the ORR activities of carbon materials. The NHPC4-700 catalyst exhibits a great catalytic performance with onset potential at 0.90 V and limiting current density of -6.0 mA cm⁻². Meanwhile, the *i*-*t* curves showed NHPC4-700 (76.1%) had better stability than that of Pt/C (70.6%) toward ORR after 15000 s. The result of methanol resistance proves that NHPC4-700 has an excellence methanol tolerance than that of Pt/C. The superior ORR electrocatalytic performance of NHPC4-700 can be ascribed to the following factors: (i) hierarchical porous structure suitable for the mass transfer; (ii) rich defects and high specific area exposing nitrogen active sites; (iii) dominant pyridinic-N and pyrrolic-N content. In conclusion, the NHPC catalyst can be a promising ORR electrocatalyst.

Acknowledgments

The authors appreciate support by the Shenzhen Basic Research Program (JCYJ20190808141611189), Basic and Applied Research Fund of Guangdong Province (2020A1515011018). Thanks for TEM measurement help of Instrumental Analysis Center of Shenzhen University (Xili Campus).

Supplementary Information: The online version of this article (<https://doi.org/10.1007/s10854-021-06049-4>).

References

1. H.B. Wu, X.W. Lou, Metal-organic frameworks and their derived materials for electrochemical energy storage and conversion: Promises and challenges. *Sci. Adv.* **3**, 1–2 (2017)
2. W.E. Winsche, K.C. Hoffman, F.J. Salzano, Hydrogen: its future role in the nation's energy economy. *Science* **180**, 1325–1332 (1973)

- J. Yang, J. Wang, L. Zhu, W. Zeng, J. Wang, Multiple hollow CeO₂ spheres decorated MnO₂ microflower as an efficient catalyst for oxygen reduction reaction. *Mater. Lett.* **234**, 331–334 (2019)
- S. Ohyagi, T. Matsuda, Y. Iseki, T. Sasaki, C. Kaito, Effects of operating conditions on durability of polymer electrolyte membrane fuel cell Pt cathode catalyst layer. *J. Power Sources* **196**, 3743–3749 (2011)
- M.W. Reed, J. Brodd, What are batteries, fuel cells, and supercapacitors? *Chem. Rev.* **104**, 4245–4270 (2004)
- Y. He, S. Hwang, D.A. Cullen, M.A. Uddin, L. Langhorst, B. Li et al., Highly active atomically dispersed CoN₄ fuel cell cathode catalysts derived from surfactant-assisted MOFs: carbon-shell confinement strategy. *Energy Environ. Sci.* **12**, 250–260 (2019)
- T. Tamaki, A. Yamauchi, T. Ito, H. Ohashi, T. Yamaguchi, The effect of methanol crossover on the cathode overpotential of DMFCs. *Fuel Cells* **11**, 394–403 (2011)
- W. Xia, R. Zou, L. An, D. Xia, S. Guo, A metal–organic framework route to in situ encapsulation of Co@Co₃O₄@C core@bshell nanoparticles into a highly ordered porous carbon matrix for oxygen reduction. *Energy Environ. Sci.* **8**, 568–576 (2015)
- Y. Li, S. Zheng, X. Liu, P. Li, L. Sun, R. Yang et al., Conductive microporous covalent triazine-based framework for high-performance electrochemical capacitive energy storage. *Angew. Chem. Int. Ed.* **57**, 7992–7996 (2018)
- K. Babel, K. Jurewicz, KOH activated carbon fabrics as supercapacitor material. *J. Phys. Chem. Solids* **65**, 275–280 (2004)
- S.G. Peera, A.K. Sahu, A. Arunchander, S.D. Bhat, J. Karthikeyan, P. Murugan, Nitrogen and fluorine co-doped graphite nanofibers as high durable oxygen reduction catalyst in acidic media for polymer electrolyte fuel cells. *Carbon* **93**, 130–142 (2015)
- X. Qiao, S. Liao, G. Wang, R. Zheng, H. Song, X. Li, Simultaneous doping of nitrogen and fluorine into reduced graphene oxide: a highly active metal-free electrocatalyst for oxygen reduction. *Carbon* **99**, 272–279 (2016)
- Y. Zhao, J. Wan, H. Yao, L. Zhang, K. Lin, L. Wang et al., Few-layer graphdiyne doped with sp-hybridized nitrogen atoms at acetylenic sites for oxygen reduction electrocatalysis. *Nat. Chem.* **10**, 924–931 (2018)
- T. Gunji, K. Sakai, Y. Suzuki, S. Kaneko, T. Tanabe, F. Matsumoto, Enhanced oxygen reduction reaction on Pt/Pb ordered intermetallic nanoparticle/TiO₂/carbon black in acidic aqueous solutions. *Catal. Commun.* **61**, 1–5 (2015)
- Ç. Güldür, S. Güneş, Carbon supported Pt-based ternary catalysts for oxygen reduction in PEM fuel cells. *Catal. Commun.* **12**, 707–711 (2011)
- N. Tachibana, Y. Yukawa, S. Somekawa, K. Shimano, La_{0.4}Ca_{0.6}Mn_{0.9}Fe_{0.1}O₃ nanoparticle-dispersed nitrogen-doped porous carbon composite as an efficient oxygen reduction electrocatalyst. *Catal. Commun.* **131**, (2019)
- S. Jiang, Y. Sun, H. Dai, J. Hu, P. Ni, Y. Wang et al., Nitrogen and fluorine dual-doped mesoporous graphene: a high-performance metal-free ORR electrocatalyst with a super-low HO₂ yield. *Nanoscale* **7**, 10584–10589 (2015)
- D. Li, Y. Jia, G. Chang, J. Chen, H. Liu, J. Wang et al., A defect-driven metal-free electrocatalyst for oxygen reduction in acidic electrolyte. *Chemistry* **4**, 2345–2356 (2018)
- P. Bober, M. Trchová, Z. Morávková, J. Kovářová, I. Vulić, N. Gavrilov et al., Phosphorus and nitrogen-containing carbons obtained by the carbonization of conducting polyaniline complex with phosphites. *Electrochim. Acta* **246**, 443–450 (2017)
- M. Beermann, E. Holtz, E. Padgett, J.F. De Araujo, D.A. Muller, P. Strasser, Real-time imaging of activation and degradation of carbon supported octahedral Pt–Ni alloy fuel cell catalysts at the nanoscale using in situ electrochemical liquid cell STEM. *Energy Environ. Sci.* **12**, 2476–2485 (2019)
- H. Wang, A. Kong, Mesoporous fluorine-doped carbon as efficient cathode material for oxygen reduction reaction. *Mater. Lett.* **136**, 384–387 (2014)
- C. Wang, F. Yang, C. Xu, Y. Cao, H. Zhong, Y. Li, Sulfur-doped porous graphene frameworks as an efficient metal-free electrocatalyst for oxygen reduction reaction. *Mater. Lett.* **214**, 209–212 (2018)
- Y. Zan, Z. Zhang, H. Liu, M. Dou, F. Wang, Nitrogen and phosphorus co-doped hierarchically porous carbons derived from cattle bones as efficient metal-free electrocatalysts for the oxygen reduction reaction. *J. Mater. Chem. A* **5**, 24329–24334 (2017)
- S. Zinatloo-Ajabshir, M.S. Morassaei, O. Amiri, M. Salavati-Niasari, Green synthesis of dysprosium stannate nanoparticles using *Ficus carica* extract as photocatalyst for the degradation of organic pollutants under visible irradiation. *Ceram. Int.* **46**, 6095–6107 (2020)
- S. Zinatloo-Ajabshir, S.A. Heidari-Asil, M. Salavati-Niasari, Recyclable magnetic ZnCo₂O₄-based ceramic nanostructure materials fabricated by simple sonochemical route for effective sunlight-driven photocatalytic degradation of organic pollution. *Ceram. Int.* **47**, 8959–8972 (2021)
- S. Zinatloo-Ajabshir, S. Mortazavi-Derazkola, M. Salavati-Niasari, Schiff-base hydrothermal synthesis and characterization of Nd₂O₃ nanostructures for effective photocatalytic degradation of eriochrome black T dye as water contaminant. *J. Mater. Sci* **28**, 17849–17859 (2017)

27. S. Zinatloo-Ajabshir, Z. Salehi, M. Salavati-Niasari, Green synthesis of $\text{Dy}_2\text{Ce}_2\text{O}_7$ ceramic nanostructures using juice of *Punica granatum* and their efficient application as photocatalytic degradation of organic contaminants under visible light. *Ceram. Int.* **44**, 3873–3883 (2018)
28. S. Zinatloo-Ajabshir, M. Salavati-Niasari, Facile synthesis of nanocrystalline neodymium zirconate for highly efficient photodegradation of organic dyes. *J. Mol. Liq.* **243**, 219–226 (2017)
29. Y. Xie, C. Zhang, X. He, J.-W. Su, T. Parker, T. White et al., Copper-promoted nitrogen-doped carbon derived from zeolitic imidazole frameworks for oxygen reduction reaction. *Appl. Surf. Sci.* **464**, 344–350 (2019)
30. L. Zhang, Y. Hu, J. Chen, W. Huang, J. Cheng, Y. Chen, A novel metal organic framework-derived carbon-based catalyst for oxygen reduction reaction in a microbial fuel cell. *J. Power Sources* **384**, 98–106 (2018)
31. L. Zhang, Z. Su, F. Jiang, L. Yang, J. Qian, Y. Zhou et al., Highly graphitized nitrogen-doped porous carbon nanopolyhedra derived from ZIF-8 nanocrystals as efficient electrocatalysts for oxygen reduction reactions. *Nanoscale* **6**, 6590–6602 (2014)
32. H. Park, S. Oh, S. Lee, S. Choi, M. Oh, Cobalt- and nitrogen-codoped porous carbon catalyst made from core-shell type hybrid metal-organic framework (ZIF-L@ZIF-67) and its efficient oxygen reduction reaction (ORR) activity. *Appl. Catal. B* **246**, 322–329 (2019)
33. S. Zinatloo-Ajabshir, M. Baladi, M. Salavati-Niasari, Enhanced visible-light-driven photocatalytic performance for degradation of organic contaminants using PbWO_4 nanostructure fabricated by a new, simple and green sonochemical approach. *Ultrason. Sonochem.* **72**, (2021)
34. L. Wang, K. Liang, L. Deng, Y.-N. Liu, Protein hydrogel networks: a unique approach to heteroatom self-doped hierarchically porous carbon structures as an efficient ORR electrocatalyst in both basic and acidic conditions. *Appl. Catal. B* **246**, 89–99 (2019)
35. F. Zhou, G. Wang, F. Huang, Y. Zhang, M. Pan, Polyaniline derived N- and O-enriched high surface area hierarchical porous carbons as an efficient metal-free electrocatalyst for oxygen reduction. *Electrochim. Acta* **257**, 73–81 (2017)
36. S. Zinatloo-Ajabshir, M. Mousavi-Kamazani, Effect of copper on improving the electrochemical storage of hydrogen in CeO_2 nanostructure fabricated by a simple and surfactant-free sonochemical pathway. *Ceram. Int.* **46**, 26548–26556 (2020)
37. M. Mousavi-Kamazani, S. Zinatloo-Ajabshir, M. Ghodrati, One-step sonochemical synthesis of $\text{Zn}(\text{OH})_2/\text{ZnV}_3\text{O}_8$ nanostructures as a potent material in electrochemical hydrogen storage. *J. Mater. Sci.* **31**, 17332–17338 (2020)
38. S. Zinatloo-Ajabshir, N. Ghasemian, M. Mousavi-Kamazani, M. Salavati-Niasari, Effect of zirconia on improving NO_x reduction efficiency of $\text{Nd}_2\text{Zr}_2\text{O}_7$ nanostructure fabricated by a new, facile and green sonochemical approach. *Ultrason. Sonochem.* **71**, (2021)
39. J. Wang, S. Kaskel, KOH activation of carbon-based materials for energy storage. *J. Mater. Chem. A* **22**, 23710–23725 (2012)
40. J. Zhang, Y. Sun, J. Zhu, Z. Kou, P. Hu, L. Liu et al., Defect and pyridinic nitrogen engineering of carbon-based metal-free nanomaterial toward oxygen reduction. *Nano Energy* **52**, 307–314 (2018)
41. F. Wang, H.R. Fu, Y. Kang, J. Zhang, A new approach towards zeolitic tetrazolate-imidazolate frameworks (ZTIFs) with uncoordinated N-heteroatom sites for high CO_2 uptake. *Chem. Commun.* **50**, 12065–12068 (2014)
42. J. Zou, P. Liu, L. Huang, Q. Zhang, T. Lan, S. Zeng et al., Ultrahigh-content nitrogen-decorated nanoporous carbon derived from metal organic frameworks and its application in supercapacitors. *Electrochim. Acta* **271**, 599–607 (2018)
43. C. Chen, M. Liu, H. Rao, Y. Liu, S. Lin, J.-K. Sun et al., Doped porous carbon nanostructures with N-Co-O catalytic active sites for efficient electrocatalytic oxygen reduction reaction. *Appl. Surf. Sci.* **463**, 386–394 (2019)
44. R.S.D. Guo, C. Akiba, S. Saji, T. Kondo, J. Nakamura, Active sites of nitrogen-doped carbon materials for oxygen reduction reaction clarified using model catalysts. *Science* **351**, 361–365 (2016)
45. Y. Zhao, X. Li, X. Jia, S. Gao, Why and how to tailor the vertical coordinate of pore size distribution to construct ORR-active carbon materials? *Nano Energy* **58**, 384–391 (2019)

Publisher's Note Springer Nature remains neutral with regard to jurisdictional claims in published maps and institutional affiliations.